PCCP

ROYAL SOCIETY OF CHEMISTRY

PAPER

View Article Online
View Journal | View Issue

Cite this: *Phys. Chem. Chem. Phys.*, 2026, **28**, 7008

The optoelectronic properties of group IV nanoparticles

Eimear Madden and Martijn A. Zwijnenburg *

We use time-dependent density functional theory and many-body perturbation theory to compare and contrast the electronic and optical properties of hydrogen capped carbon, silicon and germanium group IV nanoparticles. Hydrogen-capped silicon nanoparticles are model systems for quantum confinement and hence it is an interesting question if carbon and germanium nanoparticles similarly behave as archetypes of quantum confinement. We find that for several properties, such as the trends in the fundamental and optical gaps with particle size, all group IV systems behave similarly. However, there are also other properties, such as the variation of the electron affinity with particle size and the electronic character of the low-energy excitons and frontier quasiparticle states, for which the carbon particles behave fundamentally differently from their silicon and germanium counterparts and deviate from the idealised cartoon picture of quantum confinement. We speculate that the fact that hydrogen is more electropositive than carbon, and more electronegative than silicon and germanium, combined with the large gap of the carbon nanoparticles, pushes the unoccupied C–H σ-bonds into the gap, which then pins the lowest unoccupied quasiparticle state and excited electron component of the excitons on the surface.

Received 4th September 2025,
Accepted 2nd February 2026

DOI: 10.1039/d5cp03420e

rsc.li/pccp

Introduction

Nanoparticles with the diamond structure and capped with hydrogen atoms or organic groups have been synthesized for carbon,[1,2] silicon,[3] and germanium,[4,5] and in the case of carbon, diamondoid, nanoparticles even form naturally under geological conditions and as a result have been isolated from crude oil.[6] These group IV diamond nanoparticles find application in bioimaging and sensing and have been proposed as suitable materials for light emitting diodes, lasers, low-*k* dielectrics, photocathodes, solar-cells and data storage.[5,7,8]

Silicon nanoparticles are model systems for quantum confinement. Their lowest optical excited states (excitons) and highest occupied and lowest unoccupied quasiparticle states (states corresponding to the removal or addition of an electron) are predicted to be delocalised over the particle volume.[9] Their fundamental gap, optical gap and exciton binding energy values (see Fig. 1 for definitions) are predicted to blue shift with decreasing particle size,[9–17] as does the experimentally measured photoluminescence signal.[18,19] As such, it is interesting to understand how switching the composition of the particles changes this picture. Do carbon and germanium nanoparticles similarly behave as archetypes of quantum confinement?

Department of Chemistry, University College London, 20 Gordon Street, London, WC1H 0AJ, UK. E-mail: m.zwijnenburg@ucl.ac.uk

Ab initio calculations are ideal for answering such questions about the electronic and optical properties of nanomaterials as they allow for a like-for-like comparison between well-defined isostructural particles, and allow one to access information about the (de)localisation of relevant states, which is difficult to access experimentally. There is an extensive body of literature on predictions of the electronic and optical properties of silicon nanoparticles,[9,14,20–33] a smaller number of papers with predictions for carbon or germanium nanoparticles with the diamond structure,[2,5,6] and even fewer that consider in the same study nanoparticles of two or three of the group IV elements.[32,34–36] Very few of these papers report the (de)localisation of the excitons and quasiparticle states. Similarly, very few papers report the fundamental gap, optical gap and exciton binding energy values, often only reporting one or two out of three. Many papers also approximate the fundamental gap by the Kohn–Sham gap, the gap between the highest occupied and lowest unoccupied orbitals from a ground state from a ground state density functional theory (DFT) calculation, which is a severe approximation and typically leads to a significant underestimation of the true fundamental gap.

Here we use time-dependent DFT (TD-DFT) and many-body perturbation theory using the combination of the GW method and solving the Bethe–Salpeter equation to predict and compare the electronic and optical properties of the hydrogen terminated group IV nanoparticles with the diamond structure shown in Fig. 2. Many-body perturbation theory allows us to

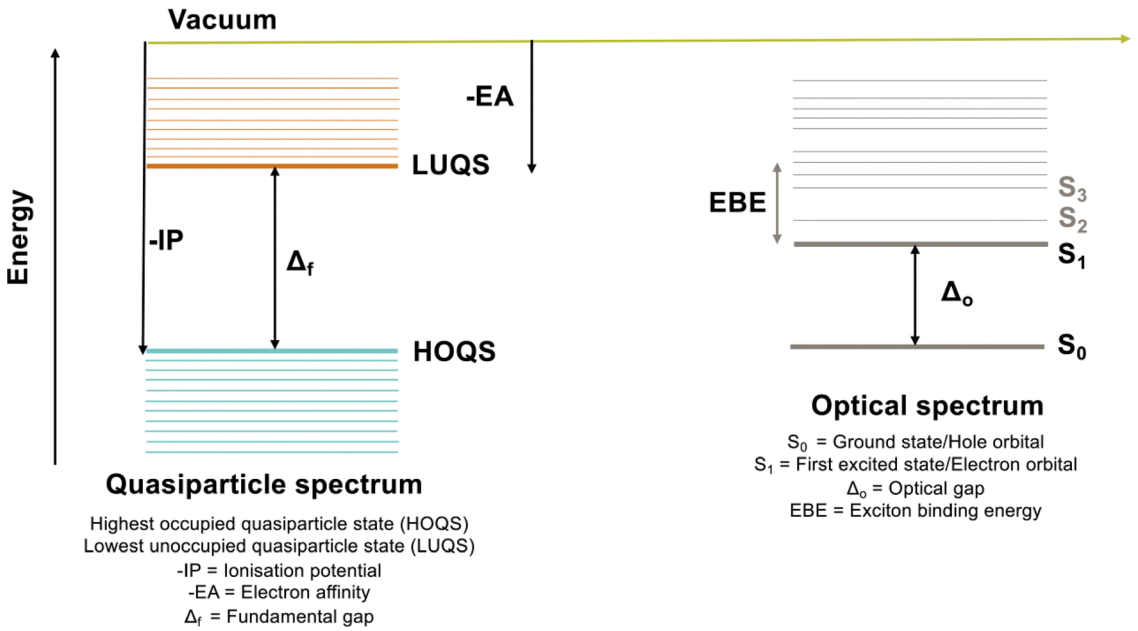

Fig. 1 Schematic representation of the quasiparticle and optical energy levels, defining the ionisation potential (IP), electron affinity (EA), fundamental gap (Δ_f), optical gap (Δ_o), and exciton binding energy (EBE), which is the difference between Δ_f and Δ_o. In this diagram, (a) denotes the highest occupied quasiparticle state, (b) the lowest unoccupied quasiparticle state, S_0 the electronic ground state, and S_1 the first singlet excited state.

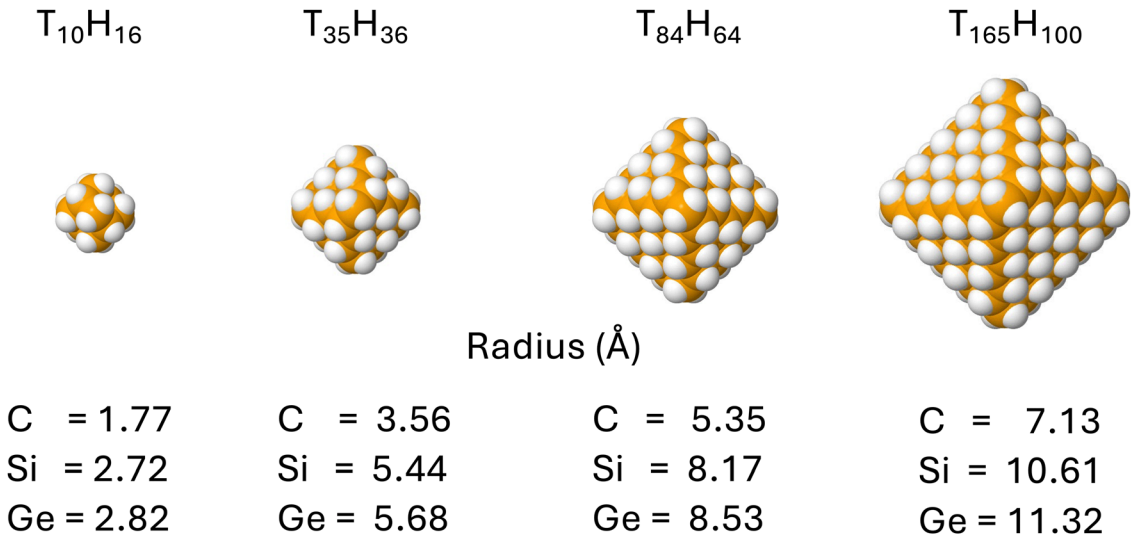

Fig. 2 DFT optimised (T_d symmetry, B3LYP and def2-SVP basis set) structures of the group IV nanoparticles studied here with their respective radii, defined *via* eqn (5) below. From left to right: $T_{10}H_{16}$, $T_{35}H_{36}$, $T_{84}H_{64}$, and $T_{165}H_{100}$, respectively, where T = C, Si or Ge.

make accurate and importantly consistent predictions of the fundamental gap, optical gap and exciton binding energy values of group IV nanoparticles while TD-DFT will allow us to extend our study to larger particles than could be studied using many-body perturbation theory. We will demonstrate that all systems considered are similar, in that the fundamental gap, optical gap and exciton binding energy increase with decreasing particle size, but in other properties the carbon nanoparticles behave rather differently from their silicon and germanium counterparts and appear less of an archetype of quantum confinement than their heavier group IV equivalents.

Methodology

Initial geometries for hydrogenated nanoparticles of silicon, carbon, and germanium were generated by making octahedral cuts from their respective bulk crystalline structures, as taken

from the Materials Project,[37] using the nanocut code,[38] and saturating the dangling bonds on the surface with hydrogen atoms. The resulting geometries were then optimised using DFT calculations employing the B3LYP hybrid functional,[39–41] augmented with Grimme's D3 dispersion correction,[42] with Becke–Johnson damping and the def2-SVP or def2-TZVP basis sets.[43] The geometries of the particles were initially optimised in their highest possible point-group (T_d), and then reoptimised in the D_2 subgroup, as well as in the absence of any imposed symmetry (C_1). The reason for the latter is that the algorithms for some of the subsequent calculations are not implemented for non-Abelian groups or cannot exploit symmetry at all. The differences between structures optimised in T_d, D_2 and C_1 were found to be minimal. Harmonic frequency calculations, performed where tractable, confirmed that the optimised structures indeed correspond to minima, displaying no imaginary frequencies.

Quasiparticle (QP) energies—including the energies of the highest occupied and lowest unoccupied quasiparticle states, the ionisation potentials, and electron affinities—were subsequently obtained from eigenvalue self-consistent GW (evGW) calculations and for the smallest particles also with quasiparticle self-consistent GW (qsGW) calculations.[44] All GW calculations used the optimised B3LYP orbitals as input and the same basis sets as used in the DFT calculations. The results of the GW calculations were also used as input for solving the Bethe–Salpeter equation (BSE) to predict vertical excitation energies, oscillator strengths, optical gaps, and static polarisabilities.[45] It is noted that evGW reduces and qsGW effectively eliminates the dependency of the GW and BSE results on the functional used in the underlying DFT calculations relative to single-shot G_0W_0 calculations by iterating the GW eigenvalues to self-consistency. Notably, in finite systems, results from evGW-BSE calculations show good agreement with coupled-cluster benchmarks, outperforming G_0W_0-BSE for singlet excitations.[46] Alternatively, time-dependent DFT (TDDFT) calculations using Tamm–Dancoff approximation were performed on each optimised nanoparticle using B3LYP and the same basis sets as for the ground state to predict vertical excitation energies, oscillator strengths and optical gaps values.[47]

All DFT, GW, and BSE calculations used version 7.5 of the Turbomole code, in combination with a tight integration grid (m5), stringent SCF convergence (DenConv set to 1×10^{-7}), and the RI-J approximation.[48–50] For the GW and BSE calculations additionally, the RI-K approximation was applied. Finally, the evGW calculations (but not the qsGW calculations) used the RIGW algorithm in which only the frontier QP states are explicitly calculated using GW and the remainder of the DFT eigenvalues just rigidly shifted accordingly. This approach scales as N^4 rather than N^6 allowing significantly larger nanoparticles to be tackled than otherwise would be possible. Because Turbomole restricts the use of non-Abelian point groups for GW and BSE, we performed these calculations in either D_2 or C_1.

Oscillator strength values are reported throughout in the velocity gauge. Characterisation of excited states was undertaken in terms of the leading natural transition orbitals (NTOs) for different excited states,[51] while the TheoDORE code was used to extract the exciton size.[52] As TheoDORE cannot handle symmetry the latter was done for results of C_1 calculations.

The effective static dielectric constants of the nanoparticles were approximated from the static polarizabilities computed in evGW-BSE. Polarizability volumes (α') were derived from raw polarisabilities (α) using the equation

$$\alpha' = \alpha/(4\pi\varepsilon_0) \quad (1)$$

Next the molecular volumes V_m of the particles were calculated using the MoloVol code and converted to the radius of an equivalent sphere r_{equiv} using

$$r_{equiv} = ((3/(4\pi))V_m)^{1/3} \quad (2)$$

And finally, the r_{equiv} values were used to approximate the static dielectric constant e_r values using

$$e_r = ({r_{equiv}}^3 + 2\alpha')/({r_{equiv}}^3 - \alpha') \quad (3)$$

The r_{equiv} values obtained from the molecular volume were used instead of a radius based on exclusively the nuclear positions, as the former takes into account the finite size of the atoms.

To examine the band-like character of the orbitals and NTOs, an in-house Python script, Fouri-yay,[53] was used to perform discrete Fourier transforms of the corresponding cube files. The Fourier transform was plotted as a function of k_x and k_y defined as

$$K_{x/y} = 2\pi/\lambda_{x/y} \quad (4)$$

with the information along the z-direction projected on the xy plane by summing up the contributions along the z-axis for each xy value.

In all property-*versus*-size plots, we use the nanoparticles' core radius R based on the average octahedral edge length, L, so that

$$R = (1/2)2^{0.5}L \quad (5)$$

Results

Fundamental gap

Fig. 3 shows the four highest occupied and four lowest unoccupied Kohn–Sham (DFT) and quasiparticle states (evGW) for each nanoparticle (carbon, silicon, and germanium), alongside their Kohn–Sham and fundamental gap values, respectively. The same data are also tabulated in Tables S1 and S10 in the SI. We observe that for each family of particles, the fundamental gap increases systematically as the nanoparticle size decreases. This is in line with what is expected from analytical models of quantum-confinement and previous computational and experimental work on silicon and germanium nanoparticles.[9,12–14,17,54] We also observe that the fundamental gap of the carbon nanoparticles is always significantly larger than their silicon and

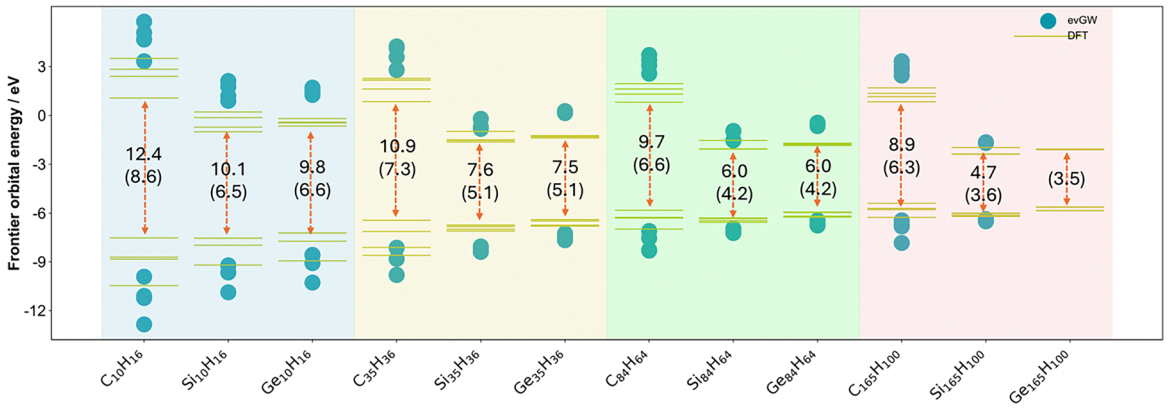

Fig. 3 Quasiparticle energy spectrum for each group IV nanoparticle, showing the four highest occupied and four lowest unoccupied Kohn–Sham orbitals/quasiparticle states, as calculated by DFT and evGW (evGW not tractable for $Ge_{165}H_{100}$). For each particle the evGW fundamental gap values are also shown with the DFT Kohn–Sham gaps given in between parentheses. All values calculated using/starting from B3LYP in combination with the def2-SVP basis set in the D_2 point group. The figure is divided by colour based on the size of the core of the nanoparticle to aid comparison where blue represents $T_{10}H_{16}$, yellow $T_{35}H_{36}$, green $T_{84}H_{64}$, and red $T_{165}H_{100}$.

germanium counterparts, which is in agreement with the bulk band gap of diamond carbon also being considerably larger than that of bulk silicon and germanium.[55–57]

In terms of the quasiparticle/Kohn–Sham state positions, the carbon nanoparticles have clearly less negative, shallower lowest unoccupied quasiparticle states than their silicon and germanium counterparts, and thus less negative (*i.e.* more positive) electron affinity values. While for each family of particles the electron affinity becomes more negative with increasing particle size, the difference in the electron affinity values between the carbon and the silicon and germanium nanoparticles actually increases with increasing particle size. In contrast, the differences between the positions of the highest occupied quasiparticle states for particles with the same size, and thus their ionisation potentials, are much smaller and the difference in ionisation potential values between the carbon and the silicon and germanium nanoparticles decreases with increasing particle size. This counterintuitive behaviour in terms of the differences between the electron affinity of the carbon and the silicon/germanium particles stems from the fact that the electron affinities of the carbon particles barely change with particle size, especially when compared to the change in the electron affinities of the silicon and germanium particles. The predicted minor change in the electron affinity values of the carbon particles with particle size agrees with the fact that the experimental preedge of the carbon K-edge absorption spectrum of diamondoid particles does not appreciably shift with particle size.[58]

DFT and evGW paint a very similar physical picture. The biggest difference is that the DFT Kohn–Sham gap is considerably smaller than the evGW fundamental gap which is related to the fact that the DFT lowest unoccupied molecular orbitals are deeper than their evGW counterparts and the DFT highest occupied molecular orbitals shallower. The underestimation of the fundamental gap when approximating it by the Kohn–Sham gap is well known and is related to the potential experienced by the occupied and unoccupied orbitals. While when using a hybrid functional the occupied and unoccupied orbitals experience a different potential, and not unphysically the same potential as in the case when using a (semi)local functional, it still isn't the correct potential of $n-1$ electrons for the unoccupied orbitals. The evGW and qsGW (Tables S9 and S16) predicted values agree well. Finally, the ionisation potential values predicted for $C_{10}H_{16}$ by evGW and qsGW agree well with the first maximum in its experimental gas phase photoelectron spectrum reported by Lenzke and co-workers.[59]

Optical gap

Fig. 4 shows the predicted optical gaps for C, Si, and Ge nanoparticles as a function of the particle size, as calculated by TDDFT and evGW-BSE. The same data are also tabulated in Tables S4 and S12 in the SI. An optical gap-size dependence is observed for all three materials, with optical gaps decreasing as the nanoparticle core grows, an outcome expected from analytical models of quantum confinement. Notably, the carbon particles exhibit consistently larger gaps than silicon and germanium for the same nominal core, consistent with its larger bulk band gap and with the fact that, as noted above, the carbon particles have consistently larger fundamental gap values than their silicon and germanium counterparts. The TD-DFT and evGW-BSE predicted optical gap values are very similar, except in the case of the carbon particles where the TD-DFT predicted gap is approximately one eV smaller than their evGW-BSE counterparts. The evGW-BSE and qsGW-BSE (Tables S9 and S16) predicted optical gap values are also very similar. Finally, the effect of basis-set size, see Tables S6, S8, S14, S15 and Fig. S2–S5 in the SI, is considerably larger for the carbon particles compared to their silicon and germanium counterparts in both TD-DFT and evGW-BSE calculations. This is similar to what was previously observed in the case of just TD-DFT by Foerster and Besley[32] (and in the case of just carbon nanoparticles by Vörös and Gali[32,60] prior to that).

The optical gap values for the silicon and germanium particles predicted by TD-DFT here are smaller than those

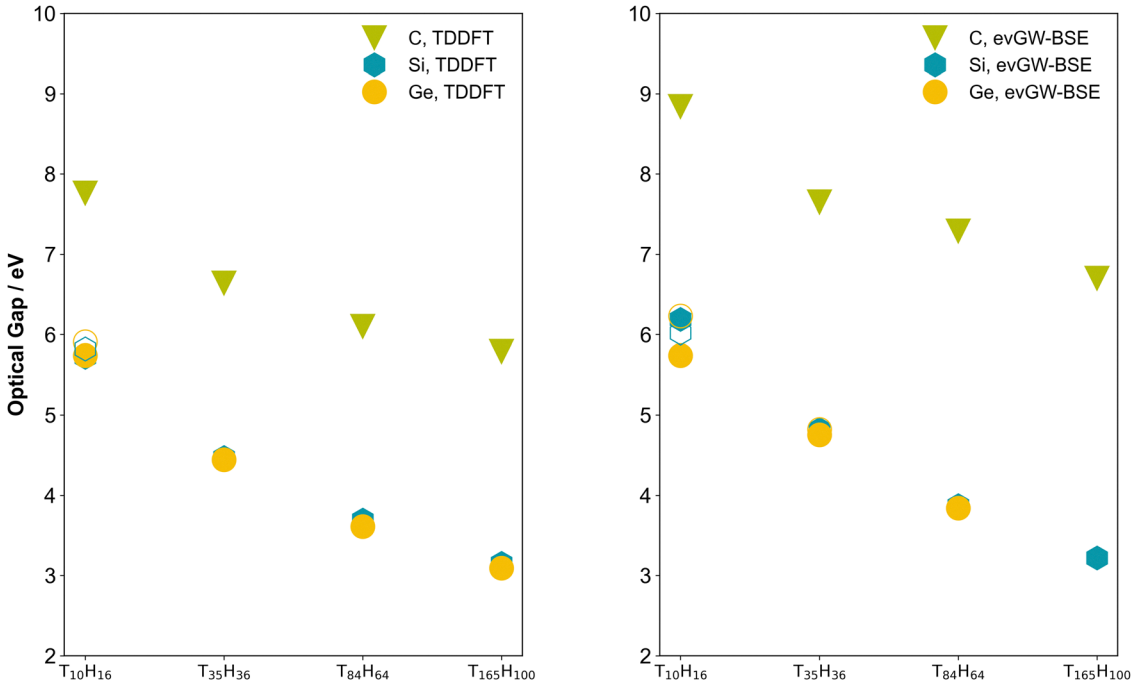

Fig. 4 Plot of optical gap *versus* particle radius for the different group IV nanoparticles, where carbon is represented by green triangles, silicon is represented by blue hexagons and germanium is represented by yellow circles, calculated using TDDFT (left panel) and evGW-BSE (right panel). All calculations use/start from the B3LYP functional and use the def2-SVP basis-set and the D_2 point group. Data in open symbols calculated using the lowest bright excited state. Fig. S2 and S3 in the SI show the same plots for different basis-set sizes.

predicted using TD-DFT by Foerster and Besley.[32] This is in line with the fact that they employed the range-separated CAM-B3LYP functional, the use of which is known to shift spectra into the blue. However, interestingly, the difference in the case of the carbon particles appears negligible, possibly because of spurious error cancellation linked to the larger effect of basis-set size for the carbon particles.

The lowest excited state of $Si_{10}H_{16}$ and $Ge_{10}H_{16}$ are non-bright and correspond to a symmetry forbidden a_2 or t_1 excitation in the T_d point group, respectively, with the lowest bright t_2 excitation lying 0.25–0.5 eV higher in energy. In contrast, the lowest excitation for $C_{10}H_{16}$ is bright and has t_2 symmetry. The lowest excited state for all other larger particles is bright or part of a quasi-degenerate pair of a bright and non-bright state. The lowest excited state for $Ge_{35}H_{36}$ is predicted to be non-bright when using evGW-BSE but bright when using TD-DFT or qsGW-BSE.

The evolution of the optical gap of particles with particle size can be fitted to the following equation:

$$\Delta_o = a + b/r^n \quad (6)$$

where a, b and n are constants. We set a to the experimental band gap, assuming negligible bulk exciton binding energy values, and fit b and n to the evGW-BSE and TD-DFT predictions. The fitted b and n values can be found in Table 1. As discussed in our previous work on silicon nanoparticles, based on simple analytical models of quantum confinement one would expect that n would change with particle size but lie in between 1 and 2. In line with what we previously observed for silicon nanoparticles, the fitted n values are considerably smaller than expected from such analytical models lying below one in all cases, except for the fit to the TD-DFT data for carbon nanoparticles. Another observation is that n generally appears to decrease and b appears to increase when going from carbon to germanium *via* silicon. This would suggest that when going larger than the particles explicitly studied here the optical gap of the carbon particles will converge much quicker to the bulk value with particle size than their silicon and especially their germanium counterparts. This is in line with the fact that the bulk Bohr exciton radius in carbon (1.5 nm),[61] is smaller than that of silicon (4.3) and especially germanium (24.3).[62]

Table 1 Fitting parameters for fits of eqn (6) to the TDDFT and evGW-BSE predicted optical gap values of different group IV nanoparticles, where a = 5.47, 1.1 and 0.8 eV for carbon, silicon and germanium respectively

Method	Material	b	n
TDDFT	C	4.52	1.16
	Ge	8.59	0.52
	Si	8.20	0.55
evGW-BSE	C	4.90	0.64
	Ge[a]	7.61	0.40
	Si	9.26	0.58

[a] Fit using 3 data points only.

Exciton binding energy

Fig. 5 plots the exciton binding energies for the different particles *versus* the particle size as calculated from the (TD-)DFT (left panel) and evGW-BSE (right panel) predicted fundamental

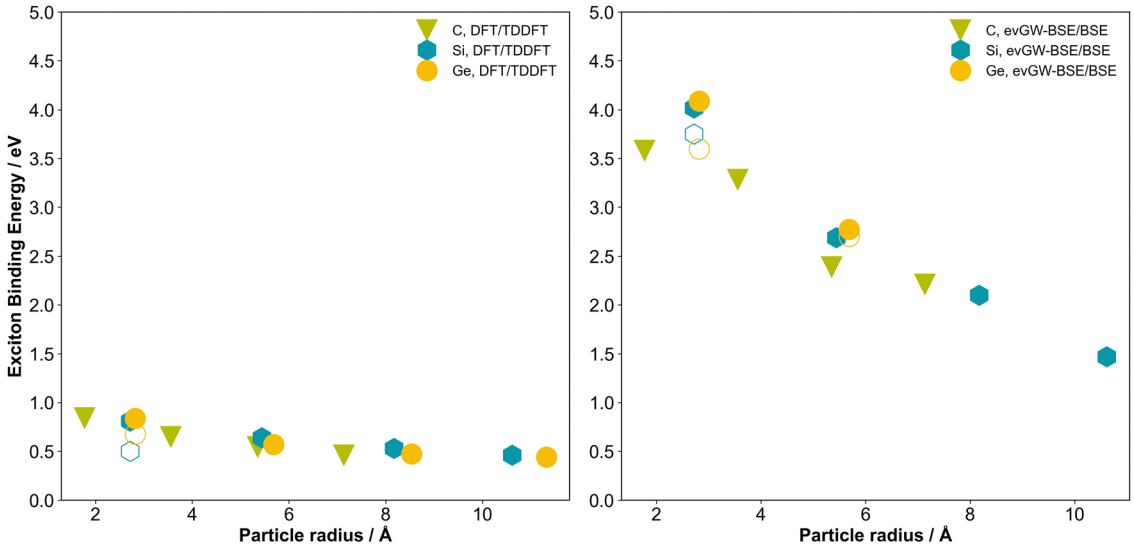

Fig. 5 Plot of the exciton binding energies *versus* particle radius for the lowest-lying excitation of the group IV nanoparticles, where carbon is represented by green triangles, silicon is represented by blue hexagons and germanium is represented by yellow circles, calculated using TDDFT (left panel) and evGW-BSE (right panel), at the def2-SVP, B3LYP level of theory under D_2 symmetry constraints. Data in open symbols calculated using the lowest bright excited state.

and optical values. From Fig. 5, it is clear that for all systems studied, the excitations corresponding to the optical gap, as well as other low-energy excitations are clearly excitonic in character. It is also interesting to note that while when the fundamental gap (Fig. S1) and optical gap (Fig. 3) are plotted against particle size, the carbon data are shifted upwards relative to their silicon and germanium counterparts but the exciton binding energy data for all group IV particles, when plotted *versus* particle size, lie more or less on a single straight line. The exciton binding energies calculated from the (TD-)DFT data are significantly smaller than those obtained from the evGW-BSE data, in line with the differences between the (TD-)DFT and evGW(-BSE) fundamental and optical gap values discussed above.

Dielectric constant

We previously demonstrated for silicon particles that these particles have a smaller static dielectric constant than bulk silicon and that the dielectric constant of the particles reduces with particle size. As a result, the dielectric screening of the particles reduces with decreasing particle size, explaining why the exciton binding energy increases with decreasing particle size. Here we estimate the dielectric constant of the $T_{35}H_{36}$ particles and find that the static dielectric constant of the particles increases in the order $C_{35}H_{36}$ (3.26) < $Si_{35}H_{36}$ (5.27) < $Ge_{35}H_{36}$ (5.90). The fact that the exciton binding energy of the group IV particles with the same number of atoms decreases when going from carbon to germanium is thus likely the result of the increasing dielectric constant down the group IV series and hence the more efficient dielectric screening. The predicted dielectric constant for $C_{35}H_{36}$ is in line with the experimental values measured for bulk powders of adamantane ($C_{10}H_{16}$), diamantane ($C_{14}H_{20}$), triamantane ($C_{18}H_{24}$) and [121]tetramantane ($C_{22}H_{28}$), which are reported to have static dielectric constant values of 2.46–2.68 compared to 5.8 for bulk diamond carbon.[8] The predicted $Si_{35}H_{36}$ dielectric constant value and the fact that it is smaller than that for bulk silicon are, as discussed in our previous work, consistent with previous more empirical calculations of the static dielectric constant of silicon nanoparticles.[63,64]

The order of the static dielectric constants of the particles is the same as that of the bulk dielectric constants of carbon (diamond), silicon and germanium, respectively.[65–68] However, the ratio of the $T_{35}H_{36}$ and bulk dielectric constants decreases when going from carbon to germanium, *i.e.*, the static dielectric constant of $C_{35}H_{36}$ is closer to that of bulk diamond carbon than that of $Ge_{35}H_{36}$ is to bulk germanium.

Real space delocalisation of the lowest excitons

Fig. 6 and 7 show the hole and excited electron components of the dominant natural transition orbitals for the different $T_{10}H_{16}$ and $T_{84}H_{64}$ particles, respectively (the latter being the largest particle size for which we can perform evGW-BSE calculations for all compositions). As can be seen, for the silicon and germanium particles the natural transition orbitals are delocalised over the volume of the particle. The picture for the carbon particles is, however, slightly different. While the hole component of the natural transition orbital for the carbon particles is delocalised over the volume of the particles, the excited electron component appears largely delocalised over just the surface of the particles. The same can also be observed for the highest occupied and lowest unoccupied orbitals in the SI (Fig. S6–S8), which serve as proxies for the highest occupied and lowest unoccupied quasiparticle states. The role of the surfaces becomes even more apparent when plotting the contribution of the group IV core and capping hydrogen atoms to the hole and excited electron component of the lowest energy

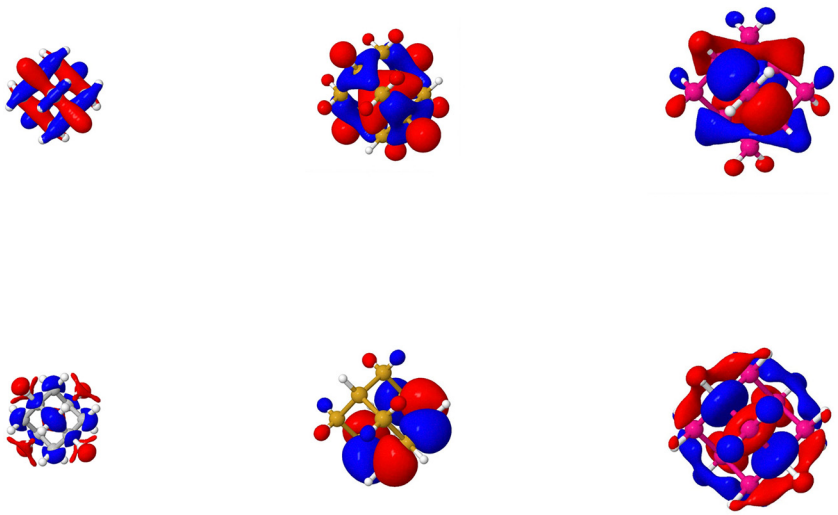

Fig. 6 Leading natural transition orbitals (NTOs) for the lowest-lying excitation of the $T_{10}H_{16}$ family where T = C (left), Si (centre), Ge (right), calculated using evGW-BSE, B3LYP and the def2-SVP basis set in the D_2 point group. Top panels display hole orbitals, and bottom panels show particle (excited electron) orbitals, with red and blue indicating the phases of the NTOs.

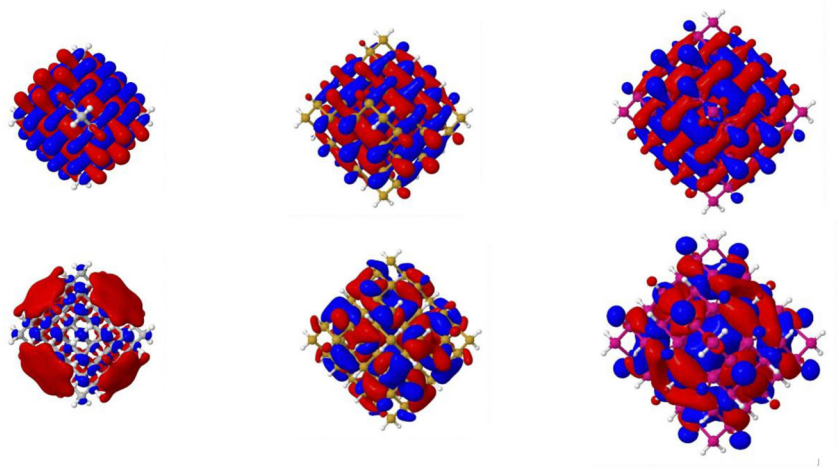

Fig. 7 Leading natural transition orbitals (NTOs) for the lowest-lying excitation of the $T_{84}H_{64}$ family where T = C (left), Si (centre), Ge (right), calculated using evGW-BSE, B3LYP and the def2-SVP basis set for the D_2 point group. Top panels display hole orbitals, and bottom panels show particle (excited electron) orbitals, with red and blue indicating the phases of the NTOs.

exciton for $T_{35}H_{36}$ particles, calculated using TheoDORE in Fig. 8. This shows that the contribution of the hydrogen capping atoms to the excited electron component is much larger than the carbon core, something that is in stark contrast to the silicon and germanium particles where the core is always the dominant contribution. For calculations using basis-sets with extra diffuse functions (def2-XVPD instead of def2-XVP) TheoDORE predicts larger contributions of the carbon core and a smaller contribution of the hydrogen atoms, even if it is still larger than that for the silicon and germanium particles. This is likely an artefact of the Löwdin charge-partition scheme used in TheoDORE, similar to the issues observed when calculating ground state Löwdin charges with basis-sets with diffuse functions.[69] The different character of the states for the carbon particles was previously observed in the literature in terms of the particle's lowest unoccupied (Kohn–Sham) orbital.[70–72] There this orbital was described as either a surface state,[71,72] or a Rydberg state.[70] We would argue that the lowest unoccupied quasiparticle state and the excited electron component of the lowest excited state of the carbon particles actually have characteristics of both a surface state (the large contribution of the surface hydrogen atoms not observed for the other group IV particles) and a Rydberg state (the large effect of basis-set size noted above, again not observed for the other group IV particles).

The delocalisation, over the particle volume and/or surface, is also apparent from Fig. 9 which shows the plot of the exciton size, defined as the root-mean-square separation between the

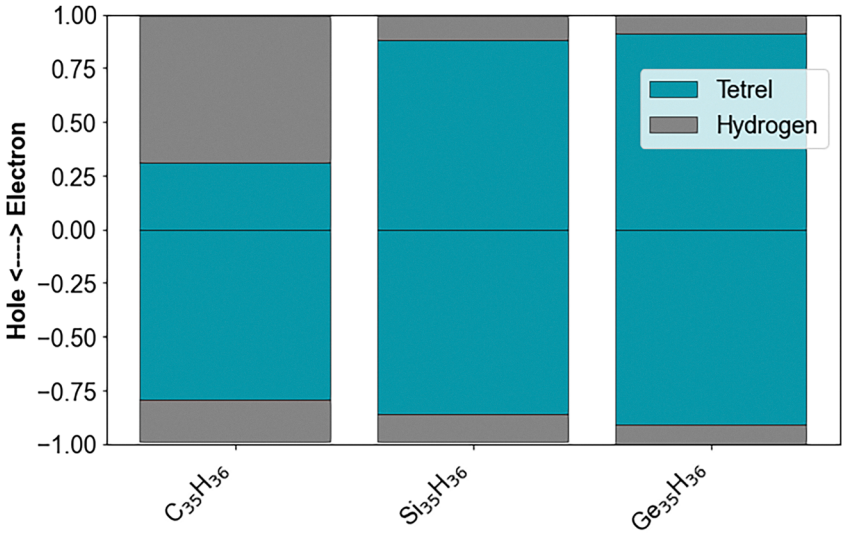

Fig. 8 Contribution of the group IV core and hydrogen capping atoms to the hole and excited electron component of the lowest exciton for $T_{35}H_{36}$. Results obtained from a TheoDORE analysis of the lowest excited states for evGW-BSE calculations on top of DFT calculations with the B3LYP functional and def2-SVP basis set.

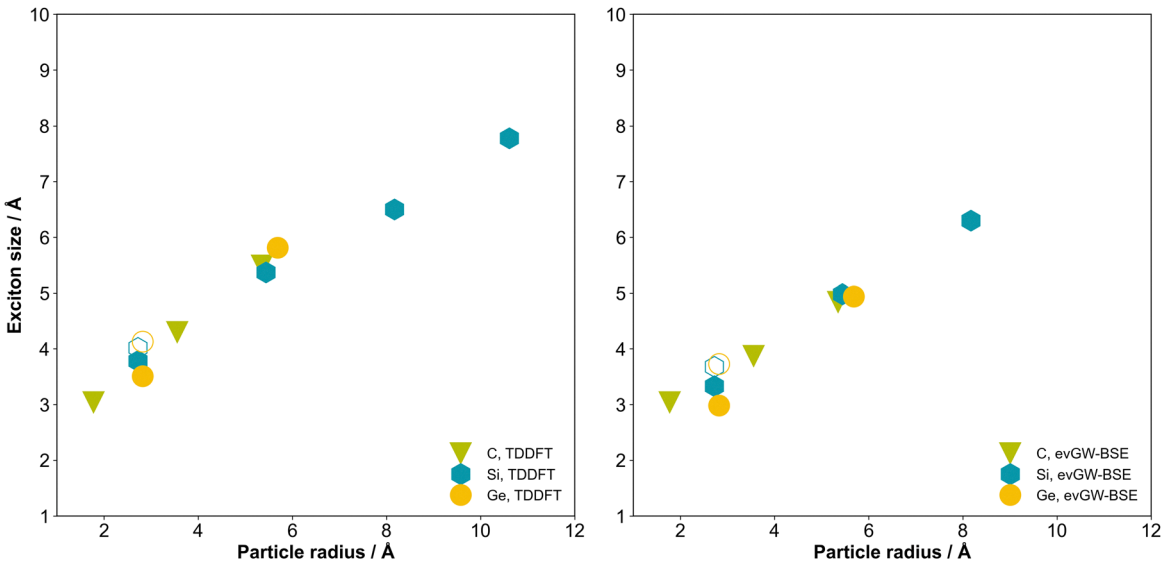

Fig. 9 Plot of the exciton size *versus* particle radius for the four smallest group IV nanoparticles, where carbon is represented by green triangles, silicon is represented by blue hexagons and germanium is represented by yellow circles, calculated using TDDFT (left panel) and evGW-BSE (right panel), and the B3LYP functional and def2-SVP basis-set in the C_1 point group.

instantaneous electron and hole position, as calculated using the TheoDORE code, *versus* the particle size and shows that for all particles the exciton size increases linearly with the particle size. Moreover, just as for the exciton binding energy, data for all systems lie on approximately the same line.

Delocalisation in reciprocal space

Finally, we studied the delocalisation of the frontier orbitals and thus the corresponding quasiparticle states by taking their Fourier transform. Fig. 10 and 11 show, respectively, the Fourier transforms for the $T_{10}H_{16}$ and $T_{165}H_{100}$ particles. In line with what we previously observed for silicon nanoparticles, for all compositions studied, the Fourier transform of the orbitals becomes sharper, less diffuse when increasing the size of the particles. Interestingly, where for the silicon and germanium particles the pattern of the maxima in the Fourier transform for the highest occupied and lowest unoccupied orbital is different, in line with the fact that the bulk materials have an indirect band gap, the pattern for the carbon particles is the same with the maxima occurring at the same k values for the highest occupied and lowest unoccupied orbitals. While one should be careful with labelling gaps as direct or indirect for

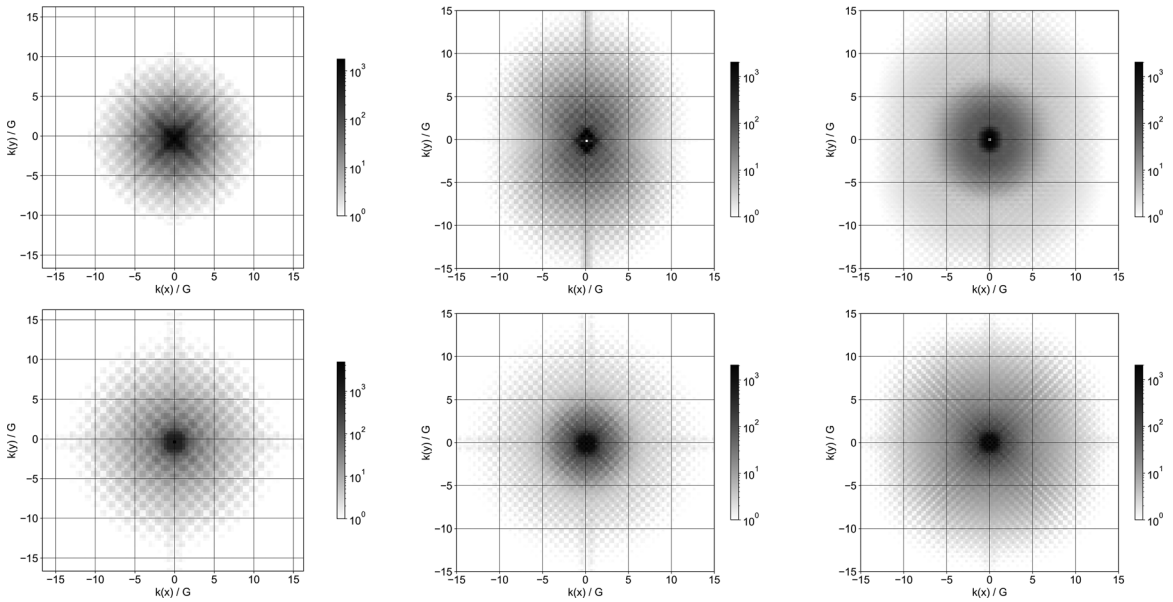

Fig. 10 Fourier transform of the highest occupied molecular orbital (top) and lowest unoccupied molecular orbital (bottom) of $C_{10}H_{16}$ (left), $Si_{10}H_{16}$ (centre) and $Ge_{10}H_{16}$ (right). Orbitals obtained using the B3LYP functional and the def2-SVP basis-set for the D_2 point group.

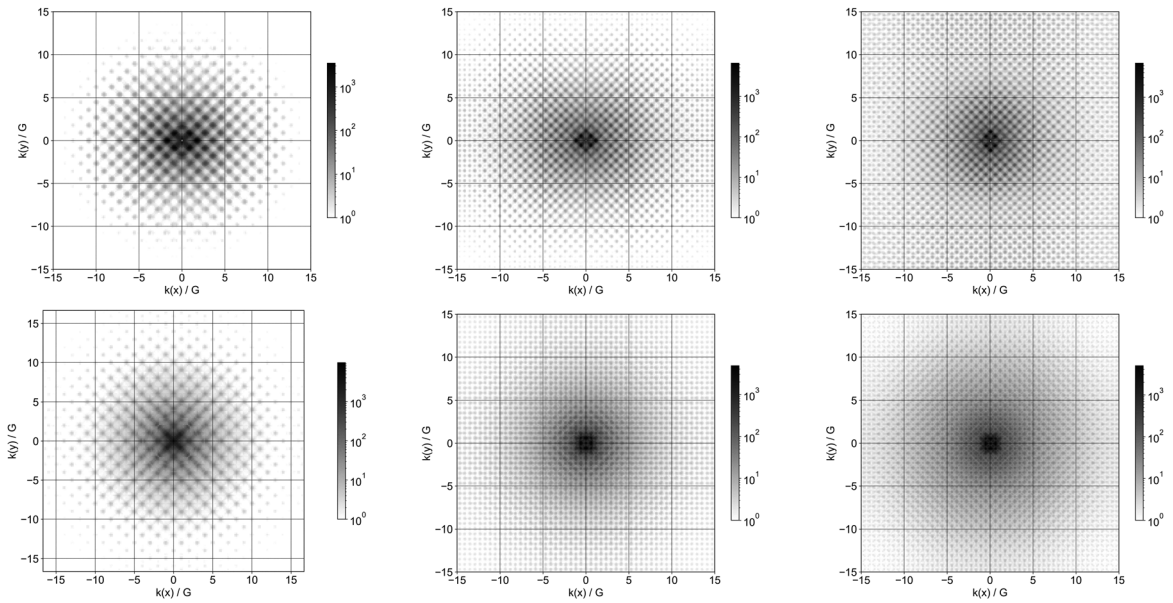

Fig. 11 Fourier transform of the highest occupied molecular orbital (top) and lowest unoccupied molecular orbital (bottom) of $C_{165}H_{100}$ (left), $Si_{165}H_{100}$ (centre) and $Ge_{165}H_{100}$ (right). Orbitals obtained using the B3LYP functional and the def2-SVP basis-set for the D_2 point group.

nanostructured systems as the wavevector k isn't a suitable quantum number in the absence of periodic boundary conditions, it is suggestive of the fact that the gap for the carbon nanoparticles has a different reciprocal space character than bulk diamond carbon and their silicon and germanium counterparts. This might be related to the different real space delocalisation of the excited-electron component of the exciton for carbon nanoparticles discussed above. It also fits with previous DFT calculations for bulk adamantane, $C_{10}H_{16}$, and related diamondoids, which predicted a direct gap for these materials.[73]

Intensities

While we do not report the predicted UV-Vis spectra of the particles here, if not only because previous work suggests that vibronic effects are significant for the spectra of diamondoid carbon nanoparticles,[74] it is interesting to note that the 'direct' fundamental gap of the carbon nanoparticles does not translate

into vertical excitations with a higher predicted oscillator strength than for the silicon and germanium particles. As can be seen from Tables S5 and S12 in the supporting information, for all group IV nanoparticles the predicted oscillator strength of the lowest energy bright excitations decreases with particle size but the values for the carbon nanoparticles are lower than their germanium (and silicon) counterparts.

Discussion

Based on the results discussed in detail above, in some aspects carbon, silicon and germanium particles behave similarly, while in other aspects, carbon nanoparticles behave rather differently to their silicon and germanium counterparts. Specifically, for all the group IV particles studied here the fundamental gap, optical gap and exciton binding energy values increase with decreasing particle size, and in real space the hole component of the excitons are similarly delocalised in real space over the particle volumes. Carbon nanoparticles are different, for example, in the fact that the electron affinity of the carbon nanoparticles does not significantly change with particle size, the contribution of the surface hydrogen atoms to the electron component of the exciton and the lowest unoccupied quasiparticle state, and the fact that the fundamental gap of the carbon nanoparticles appears 'direct' instead of 'indirect' for their silicon and germanium counterparts. From a technical perspective, key differences are also that there's a bigger disparity between the optical gap values of the carbon nanoparticles predicted using TD-DFT and those using evGW-BSE, especially compared to the silicon and germanium nanoparticles for which the predictions for TD-DFT and evGW-BSE are very close, and the larger effect of basis-set size for the carbon particles.

Inevitably, part of the differences between the carbon and silicon/germanium particles are a result of differences in the 'bulk' properties of carbon, silicon and germanium. The main examples of these would be the increased orbital overlap in carbon materials, itself linked to the shorter length of C–C bonds compared to their Si–Si and Ge–Ge counterparts, and the smaller bulk static dielectric constant of diamond carbon relative to its silicon/germanium counterparts, in turn linked to the shorter C–C bonds.[75,76] There is also, as noted above, the fact that the bulk Bohr exciton radius in diamond carbon is much smaller than that in silicon or germanium, although that is most likely a direct effect of the smaller static dielectric constant. However, it is unlikely that increased orbital overlap and/or reduced dielectric screening (alone) can explain differences, such as the contribution of the surface atoms to the lowest unoccupied quasiparticle state and excited electron component of the lowest exciton, as well as the fact that the electron affinity of the carbon nanoparticles does not significantly change with particle size. As discussed above, these phenomena have been linked in the literature to the relevant states being surface or Rydberg states for carbon particles. However, this in itself is not an explanation, as it instead raises the question of why these states are surface and/or Rydberg states for the carbon nanoparticles and not for their silicon and germanium counterparts. Replacing one question with another. We suspect that all these differences including the fact that the lowest unoccupied quasiparticle states and the excited electron component of the lowest exciton state have characteristics of surface and Rydberg states is related to the fact that hydrogen is more electropositive than carbon and more electronegative than silicon and germanium. This combined with the large gap of carbon pushes the unoccupied C–H σ-bonds into the gap, see the qualitative different character of the occupied frontier orbitals and thus the highest occupied quasiparticle states of the carbon and silicon/germanium particles, respectively, in Fig. S6–S8, and results in them primarily having hydrogen character.

The large contribution of the surface hydrogen atoms to the excited electron component of the lowest energy excitons in the carbon nanoparticles is probably the reason that even if the fundamental gap appears direct, this is in contrast to their silicon and germanium counterparts, the vertical excitations in these particles does not have higher oscillator strength (intensity) values. The delocalisation of the hole and excited electron over different parts of the particles, and the particle's volume and surface, respectively, probably reduces the real space overlap between both components, relative to their silicon and germanium counterparts where both components are delocalised over the particles' volume, and reduces the oscillator strength values.

Finally, in response to the question raised in the introduction, while germanium nanoparticles appear to be similar archetypes of quantum confinement as silicon nanoparticles, carbon nanoparticles clearly deviate from the idealised cartoon picture of quantum confinement, as illustrated by the differences discussed above.

Conclusions

We compared the optical and electronic properties of different hydrogen terminated group IV nanoparticles. We found that for all sets of particles the fundamental gap, optical gap and exciton binding energy increase with decreasing particle size, as expected from simple analytical models of quantum confinement, even if the exact scaling is slightly different from that predicted by such models. Beyond these obvious similarities we also found there to be clear differences between the carbon nanoparticles and their silicon and germanium counterparts. The electron affinity of the carbon nanoparticles does not significantly change with particle size while it does for the other group IV particles. The lowest unoccupied quasiparticle state and the excited electron component of the exciton in carbon nanoparticles are delocalised over the surface rather than the volume of the particles as they are for the silicon and germanium particles, and each displays characteristics of both surface and Rydberg states. Finally, the fundamental gap of the carbon nanoparticles appears 'direct' instead of 'indirect' for their silicon and germanium counterparts. We propose that these differences primarily stem from the fact that hydrogen is

more electropositive than carbon, and more electronegative than silicon and germanium, which, combined with the large gap of the carbon nanoparticles, pushes the unoccupied C–H σ-bonds into the gap and results in them having primarily hydrogen character. The combination then results in the (partial) pinning of the lowest unoccupied quasiparticle state and the excited electron component of the exciton in the carbon nanoparticles by the hydrogen atoms. While germanium nanoparticles appear to be similar archetypes of quantum confinement as silicon nanoparticles, carbon nanoparticles thus clearly deviate from the idealised cartoon picture of quantum confinement.

Conflicts of interest

There are no conflicts to declare.

Data availability

Supplementary information (SI): tables of GW-BSE results, supplementary figures, and DFT optimised structures of all relevant particles. See DOI: https://doi.org/10.1039/d5cp03420e.

Acknowledgements

E. M. acknowledges the UK Engineering and Physical Sciences Research Council (EPSRC) for a DTP studentship (EP/T517793/1). The authors acknowledge Junru Shen, Dr. Christof Holzer and Dr Felix Plasser for discussion.

References

1 H. Schwertfeger, A. A. Fokin and P. R. Schreiner, Prismane: a stable cage compound, *Angew. Chem., Int. Ed.*, 2008, **47**, 1022–1036.
2 J. E. P. Dahl, J. M. Moldowan, Z. Wei, P. A. Lipton, P. Denisevich, R. Gat, S. Liu, P. R. Schreiner and R. M. K. Carlson, Isolation and structure of higher diamondoids, nanometer-sized diamond molecules, *Angew. Chem., Int. Ed.*, 2010, **49**, 9881–9885.
3 K. Dohnalová, T. Gregorkiewicz and K. Kůsová, Silicon nanocrystals: surface and interface effects, *J. Phys.: Condens. Matter*, 2014, **26**, 173201.
4 D. Carolan, Silicon nanocrystals: synthesis, properties and applications, *Prog. Mater. Sci.*, 2017, **90**, 128–158.
5 B. Pescara and K. A. Mazzio, Surface chemistry of silicon nanoparticles, *Langmuir*, 2020, **36**, 11685–11701.
6 J. E. Dahl, S. G. Liu and R. M. K. Carlson, Isolation of higher diamondoids, *Science*, 2003, **299**, 96–99.
7 C. M. Gonzalez and J. G. C. Veinot, Progress toward silicon nanocrystal LEDs, *J. Mater. Chem. C*, 2016, **4**, 4836–4846.
8 W. A. Clay, T. Sasagawa, M. Kelly, J. E. Dahl, R. M. K. Carlson, N. Melosh and Z.-X. Shen, Electronic structure of diamondoids studied by photoemission spectroscopy, *Appl. Phys. Lett.*, 2008, **93**, 172901.
9 E. Madden and M. A. Zwijnenburg, Optical gaps and excitonic effects in hydrogenated silicon nanoparticles, *Phys. Chem. Chem. Phys.*, 2024, **26**, 11695–11707.
10 L. Brus, Electronic wave functions in semiconductor clusters: experiment and theory, *J. Phys. Chem.*, 1986, **90**, 2555–2560.
11 L. E. Brus, Electron–electron and electron–hole interactions in small semiconductor crystallites: the size dependence of the lowest excited electronic state, *J. Chem. Phys.*, 1984, **80**, 4403–4409.
12 B. Delley and E. F. Steigmeier, Self-consistent calculations of excited states in semiconductor microcrystals, *Phys. Rev. B:Condens. Matter Mater. Phys.*, 1993, **47**, 1397–1408.
13 J. P. Proot, C. Delerue and G. Allan, Electronic structure of semiconductor nanocrystals, *Appl. Phys. Lett.*, 1992, **61**, 1948–1950.
14 F. A. Reboredo, A. Franceschetti and A. Zunger, Self-energy corrections in semiconductor nanocrystals, *Phys. Rev. B:Condens. Matter Mater. Phys.*, 2000, **61**, 13073–13087.
15 S. Wippermann, M. Vörös, D. Rocca, A. Gali, G. Zimanyi and G. Galli, Electronic structure of silicon nanocrystals: the role of surface states, *Phys. Rev. Lett.*, 2013, **110**, 046804.
16 X. Wang, R. Q. Zhang, S. T. Lee, T. A. Niehaus and T. Frauenheim, Excitonic effects in silicon nanocrystals, *Appl. Phys. Lett.*, 2007, **90**, 123116.
17 A. Puzder, A. J. Williamson, J. C. Grossman and G. Galli, Electronic structure of silicon nanoclusters, *J. Am. Chem. Soc.*, 2003, **125**, 2786–2791.
18 M. V. Wolkin, J. Jorne, P. M. Fauchet, G. Allan and C. Delerue, Electronic states and luminescence in porous silicon quantum dots: the role of oxygen, *Phys. Rev. Lett.*, 1999, **82**, 197–200.
19 S. Furukawa and T. Miyasato, Quantum size effects on the optical band gap of microcrystalline Si–H, *Phys. Rev. B:Condens. Matter Mater. Phys.*, 1988, **38**, 5726–5729.
20 L. W. Wang and A. Zunger, Dielectric confinement effects in semiconductor nanocrystals, *J. Phys. Chem.*, 1994, **98**, 2158–2165.
21 I. Vasiliev, S. Öğüt and J. R. Chelikowsky, Electronic structure of silicon nanocrystals, *Phys. Rev. Lett.*, 2001, **86**, 1813–1816.
22 E. Degoli and S. Ossicini, Theory of silicon nanostructures, *Adv. Quantum Chem.*, 2009, **58**, 203–279.
23 F. Trani, G. Cantele, D. Ninno and G. Iadonisi, Optical properties of silicon nanocrystals, *Phys. Rev. B:Condens. Matter Mater. Phys.*, 2005, **72**, 075423.
24 E. Luppi, F. Iori, R. Magri, O. Pulci, S. Ossicini, E. Degoli and V. Olevano, Excitonic effects in silicon nanocrystals from ab initio calculations, *Phys. Rev. B:Condens. Matter Mater. Phys.*, 2007, **75**, 033303.
25 A. Gali, M. Vörös, D. Rocca, G. T. Zimanyi and G. Galli, Role of surface reconstruction in silicon nanocrystals, *Nano Lett.*, 2009, **9**, 3780–3785.
26 R. Q. Zhang, A. de Sarkar, T. A. Niehaus and T. Frauenheim, Electronic properties of silicon nanocrystals: a DFTB study, *Phys. Status Solidi B*, 2011, **249**, 401–412.
27 D. Rocca, M. Vörös, A. Gali and G. Galli, Excited-state properties of silicon nanocrystals from GW–BSE, *J. Chem. Theory Comput.*, 2014, **10**, 3290–3298.

28 A. Nurbawono, S. Liu and C. Zhang, Exciton localization in silicon nanocrystals, *J. Chem. Phys.*, 2015, **142**, 154705.
29 W. M. I. Hassan, M. P. Anantram, R. Nekovei, M. M. Khader and A. Verma, Silicon nanostructures for photovoltaic applications, *Sol. Energy*, 2016, **126**, 44–52.
30 R. Derian, K. Tokár, B. Somogyi, Á. Gali and I. Štich, Many-body effects in silicon nanocrystals, *J. Chem. Theory Comput.*, 2017, **13**, 6061–6067.
31 N. L. Matsko, Excitonic effects in ultrasmall silicon nanocrystals, *Phys. Chem. Chem. Phys.*, 2018, **20**, 24933–24939.
32 A. Foerster and N. A. Besley, Benchmarking excited-state methods for silicon nanoclusters, *J. Phys. Chem. A*, 2022, **126**, 2899–2908.
33 Y. Cho, S. J. Bintrim and T. C. Berkelbach, Excitonic structure of semiconductor nanocrystals, *J. Chem. Theory Comput.*, 2022, **18**, 3438–3446.
34 H.-Ch Weissker, J. Furthmüller and F. Bechstedt, Electronic band structure of semiconductor nanocrystals, *Phys. Rev. B:Condens. Matter Mater. Phys.*, 2002, **65**, 155328.
35 L. E. Ramos, H.-Ch Weissker, J. Furthmüller and F. Bechstedt, Optical properties of semiconductor clusters, *Phys. Status Solidi B*, 2005, **242**, 3053–3063.
36 S. Ossicini, M. Amato, R. Guerra, M. Palummo and O. Pulci, Optical properties of silicon nanostructures: a review, *Nanoscale Res. Lett.*, 2010, **5**, 1637–1649.
37 A. Jain, S. P. Ong, G. Hautier, W. Chen, W. D. Richards, S. Dacek, S. Cholia, D. Gunter, D. Skinner, G. Ceder and K. A. Persson, The Materials Project: a materials genome approach to accelerating materials innovation, *APL Mater.*, 2013, **1**, 011002.
38 B. Aradi, Nanocut, https://github.com/aradi/nanocut.
39 A. D. Becke, Density-functional thermochemistry. III. The role of exact exchange, *J. Chem. Phys.*, 1993, **98**, 5648–5652.
40 C. Lee, W. Yang and R. G. Parr, Development of the Colle–Salvetti correlation-energy formula into a functional of the electron density, *Phys. Rev. B:Condens. Matter Mater. Phys.*, 1988, **37**, 785–789.
41 P. J. Stephens, F. J. Devlin, C. F. Chabalowski and M. J. Frisch, *Ab initio* calculation of vibrational absorption and circular dichroism spectra using density functional force fields, *J. Phys. Chem.*, 1994, **98**, 11623–11627.
42 S. Grimme, J. Antony, S. Ehrlich and H. Krieg, A consistent and accurate ab initio parametrization of density functional dispersion correction (DFT-D), *J. Chem. Phys.*, 2010, **132**, 154104.
43 F. Weigend and R. Ahlrichs, Balanced basis sets of split valence, triple zeta valence and quadruple zeta valence quality, *Phys. Chem. Chem. Phys.*, 2005, **7**, 3297–3305.
44 D. Golze, M. Dvorak and P. Rinke, Fully self-consistent GW calculations, *Front. Chem.*, 2019, **7**, 377.
45 K. Krause and W. Klopper, Efficient correlation methods for excited states, *J. Comput. Chem.*, 2017, **38**, 383–388.
46 X. Gui, C. Holzer and W. Klopper, Accurate excited-state calculations using coupled-cluster methods, *J. Chem. Theory Comput.*, 2018, **14**, 2127–2136.
47 J. C. Taylor, Tamm-Dancoff Method, *Phys. Rev.*, 1954, **95**, 1313–1317.
48 F. Furche, R. Ahlrichs, C. Hättig, W. Klopper, M. Sierka and F. Weigend, Turbomole: a modular program suite for ab initio quantum-chemical and condensed-matter simulations, *WIREs Comput. Mol. Sci.*, 2014, **4**, 91–100.
49 Y. J. Franzke, C. Holzer, J. H. Andersen, T. Begušić, F. Bruder, S. Coriani, F. Della Sala, E. Fabiano, D. A. Fedotov, S. Fürst, S. Gillhuber, R. Grotjahn, M. Kaupp, M. Kehry, M. Krstić, F. Mack, S. Majumdar, B. D. Nguyen, S. M. Parker, F. Pauly, A. Pausch, E. Perlt, G. S. Phun, A. Rajabi, D. Rappoport, B. Samal, T. Schrader, M. Sharma, E. Tapavicza, R. S. Treß, V. Voora, A. Wodyński, J. M. Yu, B. Zerulla, F. Furche, C. Hättig, M. Sierka, D. P. Tew and F. Weigend, Recent advances in excited-state electronic structure theory, *J. Chem. Theory Comput.*, 2023, **19**, 6859–6890.
50 S. G. Balasubramani, G. P. Chen, S. Coriani, M. Diedenhofen, M. S. Frank, Y. J. Franzke, F. Furche, R. Grotjahn, M. E. Harding, C. Hättig, A. Hellweg, B. Helmich-Paris, C. Holzer, U. Huniar, M. Kaupp, A. Marefat Khah, S. Karbalaei Khani, T. Müller, F. Mack, B. D. Nguyen, S. M. Parker, E. Perlt, D. Rappoport, K. Reiter, S. Roy, M. Rückert, G. Schmitz, M. Sierka, E. Tapavicza, D. P. Tew, C. van Wüllen, V. K. Voora, F. Weigend, A. Wodyński and J. M. Yu, TURBOMOLE: today and tomorrow, *J. Chem. Phys.*, 2020, **152**, 184107.
51 R. L. Martin, Natural transition orbitals, *J. Chem. Phys.*, 2003, **118**, 4775–4777.
52 F. Plasser, TheoDORE: a toolbox for a detailed and automated analysis of electronic excited states, *J. Chem. Phys.*, 2020, **152**, 084108.
53 E. Madden, Fouri-yay, 2023, 202310.5281/zenodo.10377882.
54 O. Lehtonen, D. Sundholm and T. Vänskä, Time-dependent density functional theory and optical properties of molecules, *Phys. Chem. Chem. Phys.*, 2008, **10**, 4535–4550.
55 C. D. Clark, P. J. Dean and P. V. Harris, Intrinsic Edge Absorption, *Proc. R. Soc. Lond. A*, 1964, **277**, 312–329.
56 W. E. Engeler, M. Garfinkel and J. J. Tiemann, Exciton states in semiconductors, *Phys. Rev.*, 1967, **155**, 693–702.
57 P. J. Collings, The hydrogenic model of excitons, *Am. J. Phys.*, 1980, **48**, 197–199.
58 T. M. Willey, C. Bostedt, T. van Buuren, J. E. Dahl, S. G. Liu, R. M. K. Carlson, L. J. Terminello and T. Möller, Photoemission from diamondoid molecules, *Phys. Rev. Lett.*, 2005, **95**, 113401.
59 K. Lenzke, L. Landt, M. Hoener, H. Thomas, J. E. Dahl, S. G. Liu, R. M. K. Carlson, T. Möller and C. Bostedt, Electronic structure of diamondoid clusters, *J. Chem. Phys.*, 2007, **127**, 083432.
60 M. Vörös and A. Gali, Electronic excitations of silicon nanocrystals, *Phys. Rev. B:Condens. Matter Mater. Phys.*, 2009, **80**, 161411.
61 M. Popov, V. Churkin, A. Kirichenko, V. Denisov, D. Ovsyannikov, B. Kulnitskiy, I. Perezhogin, V. Aksenenkov and V. Blank, Raman Spectra and Bulk Modulus of Nanodiamond in a Size Interval of 2–5 nm, *Nanoscale Res. Lett.*, 2017, **12**, 561.
62 O. Madelung, *Semiconductors: Data Handbook*, Springer Berlin Heidelberg, Berlin, Heidelberg, 2004.

63 L.-W. Wang and A. Zunger, Quantum confinement in semiconductor nanocrystals, *Phys. Rev. Lett.*, 1994, **73**, 1039–1042.
64 C. Delerue, G. Allan and M. Lannoo, Electronic structure of semiconductor microclusters, *Phys. Rev. B:Condens. Matter Mater. Phys.*, 1993, **48**, 11024–11036.
65 B. R. Nag, Optical absorption in quantum-confined systems, *Appl. Phys. Lett.*, 1994, **65**, 1938–1939.
66 W. C. Dunlap and R. L. Watters, Optical properties of diamond, *Phys. Rev.*, 1953, **92**, 1396–1397.
67 H. R. Philipp and E. A. Taft, Optical constants of diamond, *Phys. Rev.*, 1962, **127**, 159–161.
68 U. Bangert, R. Barnes, L. S. Hounsome, R. Jones, A. T. Blumenau, P. R. Briddon, M. J. Shaw and S. Öberg, Defects and luminescence in silicon nanocrystals, *Philos. Mag.*, 2006, **86**, 4757–4779.
69 S. C. North, K. R. Jorgensen, J. Pricetolstoy and A. K. Wilson, Benchmarking basis sets for excited-state calculations, *Front. Chem.*, 2023, **11**, 1152500.
70 M. Vörös and A. Gali, Electronic excitations of silicon nanocrystals, *Phys. Rev. B:Condens. Matter Mater. Phys.*, 2009, **80**, 161411.
71 L. Landt, K. Klünder, J. E. Dahl, R. M. K. Carlson, T. Möller and C. Bostedt, Photoelectron spectroscopy of diamondoids, *Phys. Rev. Lett.*, 2009, **103**, 047402.
72 N. D. Drummond, A. J. Williamson, R. J. Needs and G. Galli, Quantum Monte Carlo study of semiconductor nanocrystals, *Phys. Rev. Lett.*, 2005, **95**, 096801.
73 T. Sasagawa and Z. Shen, Electronic structure of diamond surfaces, *J. Appl. Phys.*, 2008, **93**, 179201.
74 C. E. Patrick and F. Giustino, Electron–phonon interactions and optical absorption in semiconductors, *Nat. Commun.*, 2013, **4**, 2006.
75 J. C. Phillips, Covalent Bond in Crystals. I. Elements of a Structural Theory, *Phys. Rev.*, 1968, **166**, 832–838.
76 J. C. Phillips, Dielectric Definition of Electronegativity, *Phys. Rev. Lett.*, 1968, **20**, 550–553.

